COBEM 2023 27TH INTERNATIONAL CONGRESS OF MECHANICAL ENGENEERING

ABCM Brazilian Society of Mechanical Sciences and Engineering
27th ABCM International Congress of Mechanical Engineering
December 04-08, 2023, Florianópolis-SC, Brazil

# COB-2023-0117
# THERMOMECHANICAL ANALYSIS OF WIRE ARC ADDITIVE MANUFACTURING BY FINITE ELEMENT METHOD

**Vítor Seiji Andrade Tatemoto**
**José Carlos de Carvalho Pereira**
Mechanical Analysis and Design - GRANTE, Federal University of Santa Catarina, Florianópolis, SC, CEP 88040-900, Brazil
vitor.seiji@posgrad.ufsc.br
j.c.carvalho.p@ufsc.br

**Daniel Galeazzi**
Welding and Mechatronics Institute - LABSOLDA, Federal University of Santa Catarina, Florianópolis, SC, CEP 88040-900, Brazil
daniel.galeazzi@posgrad.ufsc.br

***Abstract.*** *Wire arc additive manufacturing (WAAM) presents a way to unite the design freedom and rapid manufacturing of additive manufacturing with the high deposition rate and low feed material cost of welding technologies. However, the large amount of thermal energy and material added during metallic deposition causes residual stress and geometric distortion that can compromise the product's functionality and structural integrity. Numerical simulation using finite element method (FEM) offers a tool for stress and distortion predictions that occur during arc welding thermal cycles. In this work, a FEM model to simulate the WAAM process is proposed, in order to predict the temperature field, residual stresses and distortions in the part. The numerical simulation in a three-dimensional model of a thin wall is implemented by a transient thermal analysis coupled in series with mechanical analysis. A double ellipsoid model for heat generation on activated elements is adopted. The model evaluation is accomplished by comparing the results obtained in the part temperature field and distortion from numerical analysis and experimental tests.*

***Keywords:*** *Additive Manufacturing, Wire Arc Additive Manufacturing, Finite Element Method, Residual Stress, Distortion.*

## 1. INTRODUCTION

Additive manufacturing (AM) is considered as a major innovation of manufacturing technology in the 20th century. It can produce complex shaped parts with high accuracy as well as reduce processing cycle (Li et al., 2022). WAAM is one of the metal additive manufacturing processes that uses metal wire as feed material and arc welding as heat source, similar to traditional welding technologies. The advantages of high material deposition rates and the low cost of the feed material in WAAM stand out for allowing the use of AM in the fabrication of large and/or complex design parts. Other advantages of this method are: a) the lower energy cost of the heat source, b) the non-necessity of a metallic powder protection system, and c) the possibility of working with highly reflective metals (Li et al., 2022). Among the welding techniques, the most used in WAAM are those based on gas metal arc welding (GMAW) through dynamic wire feeding. The best-known commercial variant of the technique is CMT (Galeazzi et al., 2022). Despite the numerous advantages of WAAM, the parts manufactured by this technology are subject to thermal cycles with focused heating and partial phase changes, these effects can result in distortion and residual stresses in the part. Residual stresses can cause thermal cracking, reducing the structure fatigue life (Szost et al., 2015). Distortions can also compromise component functionality (Szost et al., 2015). Numerical simulations by FEM are presented as an effective way to predict the structure behavior, in order to anticipate its distortion and residual stresses during the manufacturing stage. In addition, numerical simulations enable to test different deposition strategies as a mean to minimize geometric and mechanical defects in the part.

The first numerical simulations of additive manufacturing process by FEM were based on numerical models of welding processes (Michaleris and DeBiccari, 1997). The most commonly applied heat source model is the Goldak's double ellipsoid model which was derived from the modeling of the welding process (Goldak et al., 1984). Other heat source models were developed aiming to simplify the FE model, thus reducing the simulation computational time (D. Ding et al., 2021). To model the deposition of material in layers the method of birth and death of elements is commonly used. Research currently attempts to find ways to optimize the consumed computational time, either through quasi-static thermal analysis (J. Ding et al., 2011), adaptive mesh (Ganeriwala et al., 2021) or inherent strain method (Murakawa et al., 2012).

This work aims to develop a thermomechanical analysis of a thin wall manufacturing by WAAM. A decoupled transient thermal simulation will be performed followed by a mechanical simulation employing the resulting temperature field. Both analyzes will be implemented by a numerical finite element model. A routine will be elaborated for both, the

elements birth and death and for the heat source within the software ANSYS. An experimental test case will be carried out in order to collect temperature and distortion during the manufacturing stage. The experimental results will be used to validate and adjust the numerical model.

## 2. PROPOSED FEM MODELING

For the thermal modeling the heat generated by mechanical strain is not considered due to its low value when compared to the welding heat source (Radaj, 1992), to this extent, it is possible to perform the thermal analysis decoupled. The temperature field is used as the loading of the mechanical analysis, as thermal expansion. The material parameters are considered temperature dependent, therefore, the influences of the material phase change are included in the temperature change. The geometry of the flat base and the thin wall and mesh division used in this work are shown in Figure 1. The analysis was considered symmetric in relation to the $YZ$ plane. The mesh is shared between both analyses.

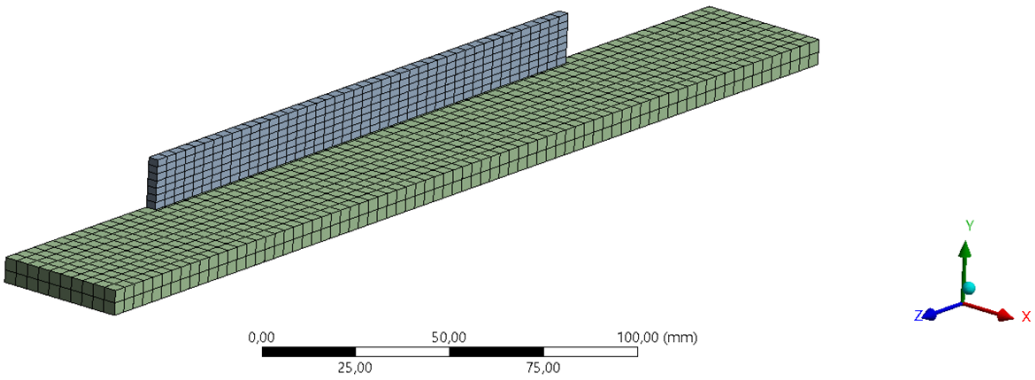


Figure 1. FE model mesh of the part.

### 2.1 Thermal modeling

The thermal modeling through a transient analysis was carried out, using the energy balance to obtain the temperature field at each time step. In AM, the use of the birth and death of elements aims to replicate the material deposition process in welding. In this work, the use of quiet elements was adopted. In quiet elements, element deactivation occurs by reducing its influence on the mesh by changing its physical properties. In the thermal simulation, the deactivation of the element occurs due to the reduction of its thermal conduction and specific heat coefficients. This reduction occurs with the use of a scale factor as represented in Eq. (1):

$$k_{quiet} = \alpha_s k, \tag{1}$$

being $k_{quiet}$ the coefficient of the inactive element, $k$ the coefficient of the active element and $\alpha$ the scale factor. The use of quiet elements is desirable because it doesn't change the number of equations in the energy balance (Lindgren, 2001). The elements belonging to the wall are deactivated at the beginning of the simulation and are activated as the heat source moves. The activation criterion of the elements is the distance between the center of the element and the center of the heat source for each time step. In this work, the activation distance was considered as half the width of the built wall. The element, when activated, has its physical properties restored.

The volumetric heat source model used in this work was the Goldak double ellipsoidal model. This model is already consolidated in the numerical analysis, and it is suitable for obtaining the temperature gradient around the heat source accurately (J. Goldak and Akhlaghi, 2005). The heat distribution equation of the double ellipsoidal model can be written as:

$$q_{f,r}(x,y,z) = \frac{6\sqrt{3}\,P f_{f,r}}{abc_{f,r}\pi\sqrt{\pi}} \exp\left(-3\frac{x^2}{a^2} - 3\frac{y^2}{b^2} - 3\frac{z^2}{c_{f,r}^2}\right), \tag{2}$$

which $P$ is the welding process power, $f$ is the distribution factor, $a$, $b$ and $c$ are the lengths of the ellipsoid axes of the volume of the heat source and $x$, $y$ and $z$ are the coordinates to be evaluated, being $z$ the welding direction. The heat distribution equation is separated into two halves. For positions in front of the heat source, the frontal coefficients are: $c_f$ and $f_f$, and for positions behind the heat source, the rear coefficients are: $c_r$ and $f_r$. The welding process power can be estimated by the electrical power equation:

$$P = IU\eta, \tag{3}$$

where $I$ is the effective current, $U$ the effective voltage and $\eta$ the efficiency of the welding process. The geometric representation of the heat source is shown in Figure 2. The heat source parameters are shown in Table 1. The parameter values were selected to replicate the fusion zone of a CMT weld.

Table 1. Heat source parameters.

| Q [W] | $a$ [mm] | $b$ [mm] | $c_f$ [mm] | $c_r$ [mm] | $f_f$ | $f_r$ |
|---|---|---|---|---|---|---|
| 2245 | 2.5 | 3.0 | 2.0 | 6.0 | 0.5 | 1.5 |

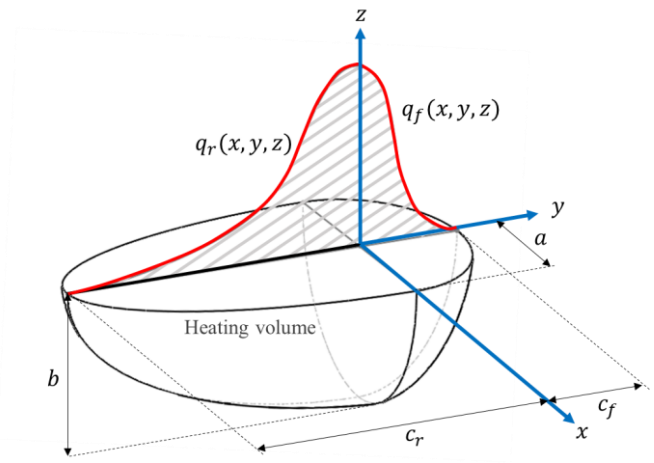


Figure 2. Heat source model.

The thermal model uses temperature-dependent physical parameters. The latent heat absorbed by the material during the phase change from solid to liquid is substantial, therefore, it is necessary to be embodied in the thermal analysis (Masubuchi, 1980). In this work, the representation of this phenomenon occurs through the increase of the specific heat value in temperatures around 700 ºC. In the weld pool, in addition to heat transfer by conduction, the material also transfers heat by convection since it is in the fluid state. The embodiment of this phenomenon occurs through the increase of the conduction coefficient for temperatures above 1000 ºC. The values for the physical parameters were obtained from the works of Montevecchi et al., (2016) and Deng, (2009). These values are shown in Table 2.

For the modeling of the initial conditions, an ambient temperature of 20 ºC was set for the base nodes. The model's boundary conditions were assumed to be natural convection on its free surfaces. Two convection coefficients were established: one for the lower surface of the base, in which there is a cooling system, and another for all other free surfaces of the part, both independent of temperature. The estimated convection coefficient for the cooled surface was 300 W/m²K. For the other free surfaces, the value of 5.7 W/m²K was obtained from the Michaleris and DeBiccari, (1997). In the plane of symmetry, it is considered that there is no heat conduction in the direction normal to the plane.

### 2.2 Mechanical modeling

The mechanical modeling was carried out through a static structural analysis, using the momentum equation to obtain the displacements and residual stresses field. The loading of the mechanical simulation occurs by the thermal expansion resulting from the temperature change, so the number of steps in the mechanical simulation is the same as the number of time steps in the thermal simulation. Hence, the nodal temperatures of each time step were transferred between both analyses. The birth and death of elements in mechanical analysis is the same used in thermal analysis, but the scale factor changes the element stiffness coefficient in the mechanical analysis.

The material was modeled with the structural physical parameters dependent of temperature. The material density was considered constant in the thermal analysis since the volume change is embodied in the material thermal expansion. At high temperatures, the low values of yield strength lead to numerical convergence problems (Lindgren, 2006), so a cut-off temperature of 700 ºC was set. Above the cut-off temperature, the yield strength was considered constant. The parameters of the wire and base material were considered the same, except for the yield strength parameter. During the welding process, the filler material undergoes melting, solidification, and annealing, therefore this process eliminates the plastic strain accumulated in the material added through the welding process (Shan et al., 2009). In this way, the equivalent plastic strain history in the recently activated elements is eliminated, also eliminating their hardening effects. The plasticity model used is the kinematic hardening model. The material constitutive parameters are shown in Table 2.

The boundary conditions used in the mechanical modeling restrict displacement in three directions at 8 points of the base, related to the physical restriction imposed by the clamps. The restriction points are shown by black squares in Figure 3. After the thermal process, the four constraints R1 are removed, replicating the releasing of the clamps. Constraints R2 to prevent rigid body movement of the part were held. In addition, a body with high rigidity under the flat base was added, in order to prevent negative vertical displacement of the part, and to allow positive vertical displacement. This high rigidity body restriction was maintained throughout the simulation. In the plane of symmetry, it is considered that there is no displacement in the normal direction to the plane.

Table 2. Material parameters.

| $T$ [ºC] | $k$ [W/mºC] | $C_p$ [J/kgºC] | $\alpha$ [$\mu$ºC$^{-1}$] | $E$ [GPa] | Wire $\sigma_Y$ [MPa] | Base $\sigma_Y$ [MPa] |
|---|---|---|---|---|---|---|
| 20 | 52 | 480 | 12.0 | 206 | 450 | 350 |
| 100 | 51 | 507 | 12.3 | 206 | 450 | 350 |
| 200 | 48 | 532 | 12.7 | 201 | 420 | 305 |
| 300 | 44 | 574 | 13.1 | 200 | 390 | 390 |
| 400 | 43 | 624 | 13.6 | 165 | 320 | 320 |
| 500 | 39 | 703 | 14.0 | 100 | 260 | 180 |
| 600 | 35 | 788 | 14.4 | 60 | 170 | 125 |
| 700 | 32 | 870 | 14.8 | 40 | 50 | 60 |
| 723 | 28 | 798 | 14.9 | 39 | 50 | 60 |
| 850 | 26 | 679 | 15.4 | 30 | 50 | 60 |
| 900 | 26 | 658 | 15.6 | 20 | 50 | 60 |
| 1250 | 30 | 666 | 16.0 | 10 | 50 | 60 |
| 1450 | 30 | 666 | 16.0 | 10 | 50 | 60 |
| 1500 | 120 | 670 | 16.0 | 10 | 50 | 60 |

## 3. EXPERIMENTAL VALIDATION

In order to check the effectiveness of the proposed numerical model, an experimental test to validate and adjust the thermal and mechanical results was carried out. The geometry and setting used in the numerical analysis aim to portray the experimental analysis. The test was performed by the additive manufacturing of a thin wall through the CMT welding process on a flat base.

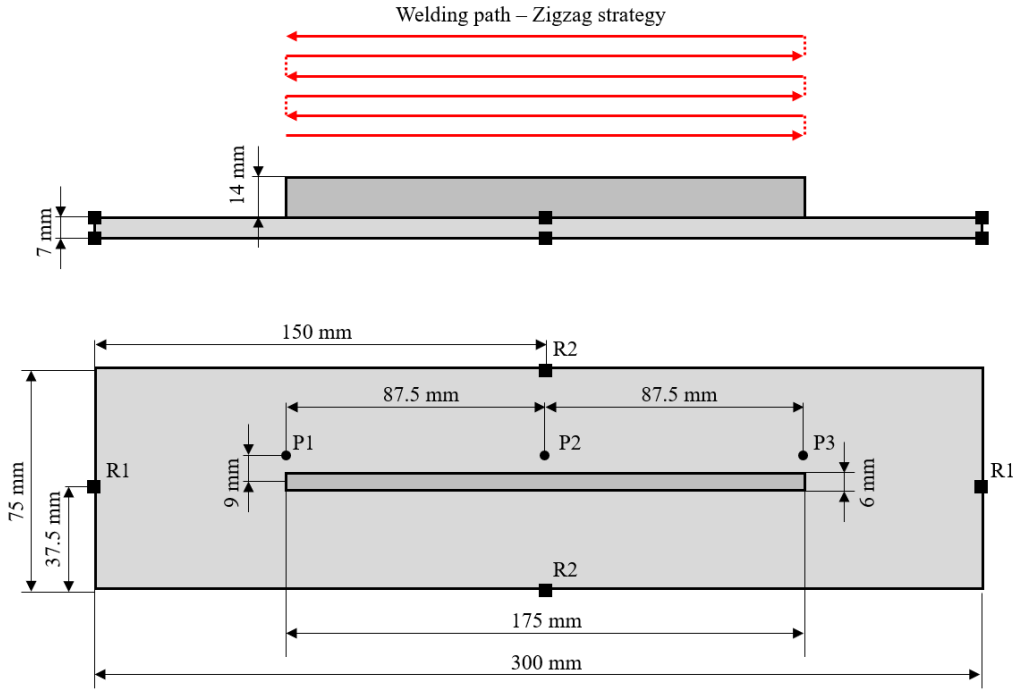


Figure 3. Design and geometry of the experimental validation.

The experiment used a carbon steel ER 70s-6 wire with a diameter of 1.2 mm. The base is made of A36 carbon steel measuring 300 x 75 mm with 7 mm thickness. The wall was built by overlapping layers in order to achieve the geometry dimensions of 6 mm width, 175 mm length and 14 mm height, through 6 layers. The schematic illustration of the geometry, welding path and measurement points are shown in Figure 3.

The welding was done with the Fronius CMT Advanced 400R welding power source and wire feeder in conjunction with a six-axis robotic arm Yaskawa Motoman HP20D. CMT welding is a variation of the GMAW method in which the material transfer mechanism occurs by immersion and retreat of the wire in the weld pool at high frequency. Current and voltage parameters are controlled by the power source in synergy with the CMT process. The CMT method was selected due to the high rate of deposition of material with low thermal input, thus reducing distortions and residual stresses in the part (D. Ding et al., 2015). The layer deposition strategy will be linear with the layers deposited in alternate directions, also called zigzag strategy. The welding travel speed was 10 mm/s and the established welding feed speed was 6 m/min. The resulted welding power was 2245 W, thus achieving a heat input of 2245 J/mm, based on a welding time of 17.5 s per layer. The efficiency coefficient of the welding process was estimated at 86% according to Arevalo and Vilarinho, (2012). The shielding gas used was C8 (92% Ar and 8% $CO_2$) with a 15 L/min flow rate and with 20 mm contact-tip-to-work-distance (CTWD). The temperature between layers was set to a maximum value of 100 ºC, being measured on the middle surface of the upper weld bead. The base support of the welding part was a water-cooled plate measuring 600X600 mm, with 1 L/min water flow at 20 ºC. The part was fixed to the water-cooled plate through 4 clamps, preventing displacement where it was fixed. Figure 4 shows the worktable with the equipment used in the manufacturing of the part including the welding torch, fastening clamps and thermocouples. The finished part made by WAAM is also shown in Figure 4.

The wall temperature measurement was performed using a FLIR SC7000 infrared camera with a 50 mm lens. The temperature range established in the camera was 300-1500 ºC. The camera was positioned at a distance of 1 m from the manufactured part. A material emissivity of 0.87 was used for thermal image analysis. The temperature measurement of the flat base was performed using 3 thermocouples, K type, and they were used as reference temperature throughout the welding process. The thermocouples were located at the points P1, P2 and P3, 9 mm from the center of the wall, presented in Figure 3. The electric current, voltage and gas flow were measured throughout the process through the SAP V4 acquisition equipment. In addition, after the removal of the fastening clamps, the distortion of different points on the upper surface of the flat base were measured in relation to the water-cooled plate surface using a caliper. The distortion measurement points are located on the sideline of the base. The test was carried out twice, the first test aiming to capture the infrared footage of the wall manufacturing, and the second test aiming to measure the temperatures and distortions of the flat base. The central clamps of the first test were removed for better acquisition of the infrared footage.

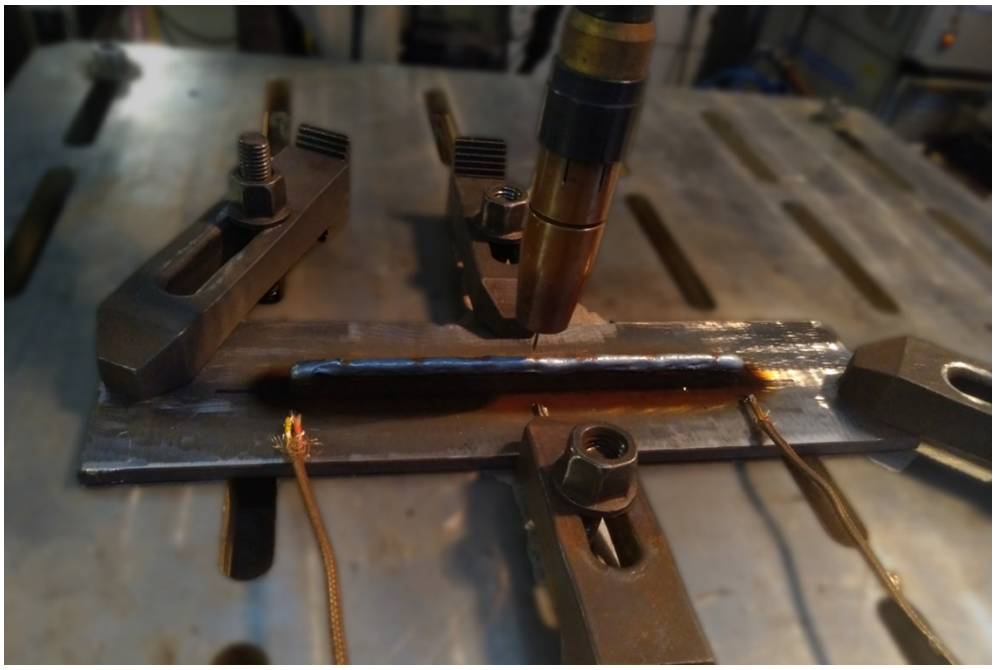

Figure 4. Working bench and the finished part.

## 4. RESULTS

Numerical analysis allows investigating the temperature in all active nodes of the mesh in each time step. Figure 5 shows the lateral view of the temperature field plot on the part during the deposition of the last layer by numerical

simulation. The figure presents the temperature gradient of the process, as well as the maximum temperature in the weld pool. It is possible to compare these results with infrared camera images of the same instant in the welding process. Figure 6 shows the lateral view of the measured surface temperature of the part during the deposition of the last layer. The outline of the expected wall geometry has been drawn in the figure for better visualization. Analyzing the image from the infrared camera, it is possible to observe that the highest temperatures are not located on the upper surface of the wall, but in a layer just below. This effect can be caused by the variation of the thermal convection coefficient on the upper surface during the layer deposition time. Another difference that can be highlighted in the infrared camera image is a region behind the heat source whose temperature is much lower than its surroundings. This effect can be explained due to the change in the emissivity of the material in the liquid phase, thus drastically decreasing the measured apparent temperature. The numerical model displays high temperatures in the region of the weld pool even with the increase of the conduction coefficient of the material for temperatures above the melting temperature. The simulation temperatures in regions of the wall far from the welding torch present results consistent with the infrared camera image.

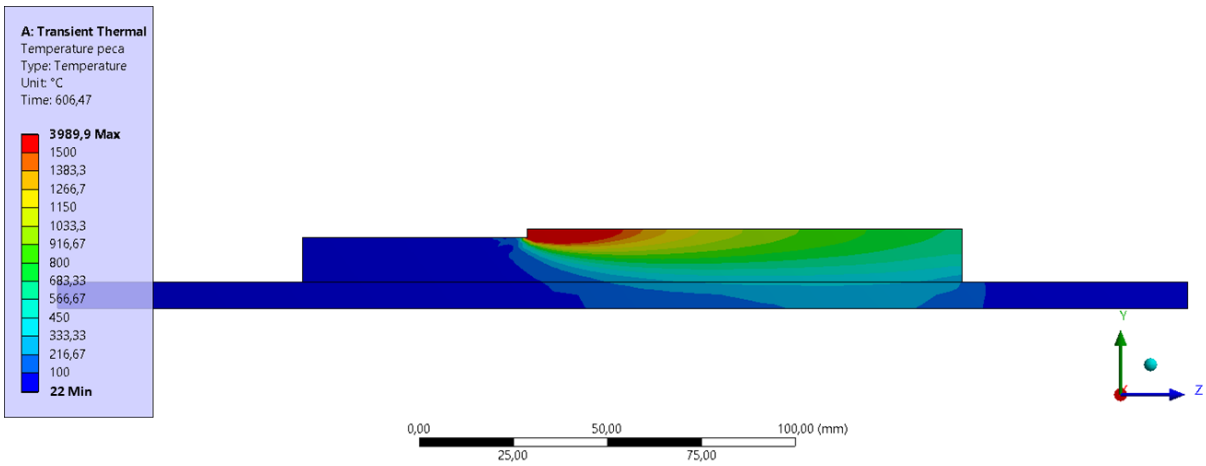


Figure 5. Temperature field of the last layer of the wall in the numerical simulation.

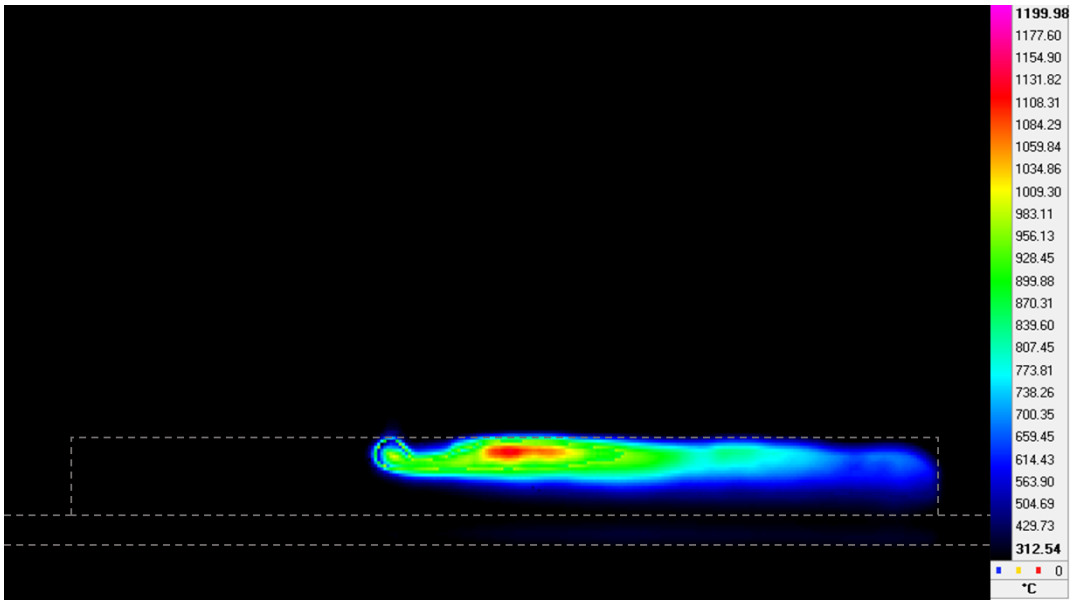


Figure 6. Temperature field of the last layer of the wall in the experimental test.

For the validation of the thermal model, the measurement of the temperature at three points, P1, P2 and P3, on the flat base during the AM process is proposed. Figure 7 shows the comparison of the temperatures measured by the thermocouples and the corresponding points in the numerical simulation during the deposition of the second layer. The predicted temperatures in the numerical simulation are in agreement with the experimentally measured temperatures. It can be noted in the temperature curves comparison that the cooling gradient of the numerical simulation is more accentuated than the experimental one. This difference may be due to the numerical modeling overestimating the heat

exchange between the base and the water-cooled plate by a convection boundary condition. With each layer deposition, the maximum temperature reached at the base dropped approximately 15 °C.

The validation of the mechanical model was carried out by comparing the distortion at the part base, at different points along the length, after releasing of the clamps. Figure 8 shows the comparison between the distortion of the experimental test and the numerical simulation. The numerical model presented distortion results in agreement to the experimental results. During the elaboration of the numerical model, it was observed that the dominant material parameter in the distortion results is the yield strength of the material. Thus, it is necessary to properly select these parameters, both for the base material and for the wire material. The proper configuration of the numerical model's movement restriction had a great influence on the results obtained.

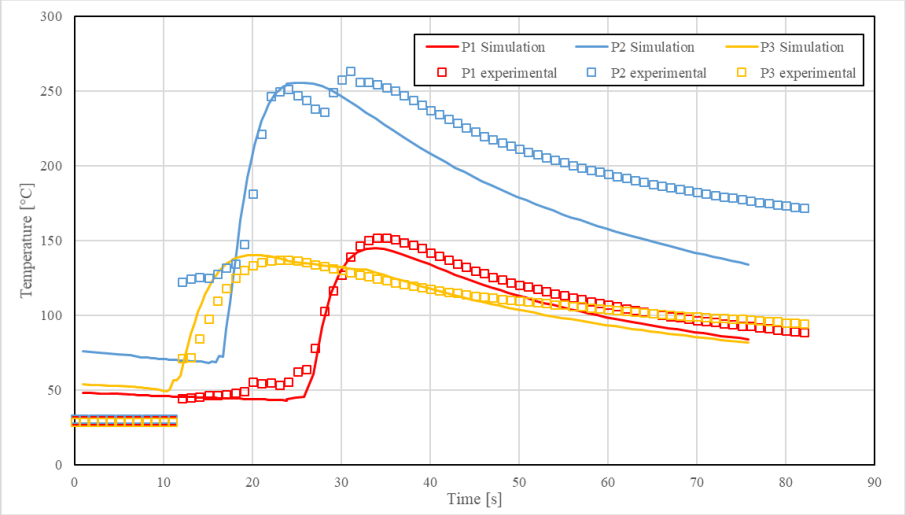


Figure 7. Comparison of thermocouple temperature history

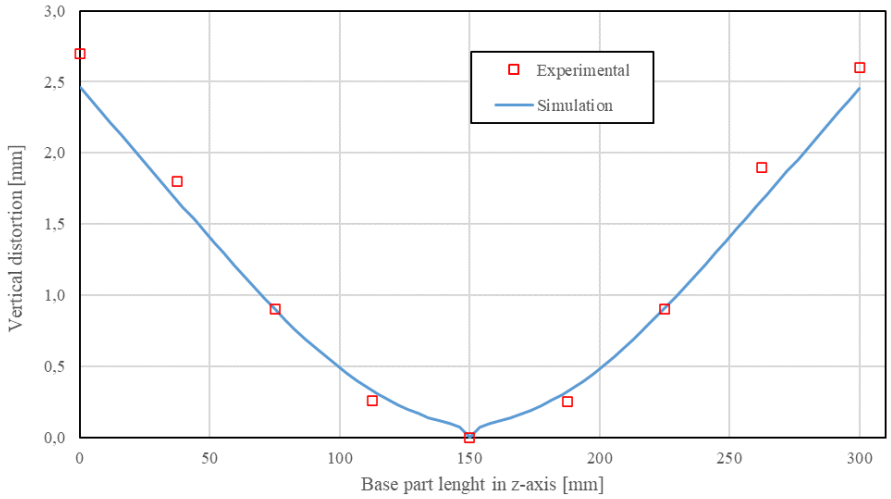


Figure 8. Distortion comparison along the sideline of the flat base

Numerical modeling enables a complete behavior analysis of the part during and after the AM. Figure 9 presents the distortions of the flat base in three-dimensions after releasing of the clamps. Figure 10 shows the longitudinal residual stress, stress normal to Z axis after the releasing of the clamps.

The residual stresses found in the numerical analysis reflect the effects of thermal expansions and contractions during welding thermal cycles. The thermal expansions are not uniform, occurring in the central region, and are contained by the colder regions farther from the center of the part. The plastic strains that occur due to stresses above the yield strength of the material, lead to residual stresses even after cooling the part. Figure 10 indicates that close to the wall, the base presents longitudinal tensile stresses, and as it moves away from the center, the longitudinal stresses become compressive. Longitudinal stresses have the highest absolute values because they are in the same orientation as the welding direction. After releasing the clamps, the predominant vertical distortions are in the longitudinal direction, also called bending

distortion, illustrated in Figure 9. This predominance is due to the direction of welding, but also to the geometry of the part base and the type of movement restriction imposed on the base. The zigzag deposition strategy is also responsible for affecting the results obtained in the longitudinal distortions. If a wider flat base was used, the transverse distortions would increase. The flat base presents, to a lesser extent, distortion in the transverse direction, also called angular shrinkage. Both analyzes are in agreement with the results obtained experimentally and make it possible to predict the mechanical defects in the part manufacturing.

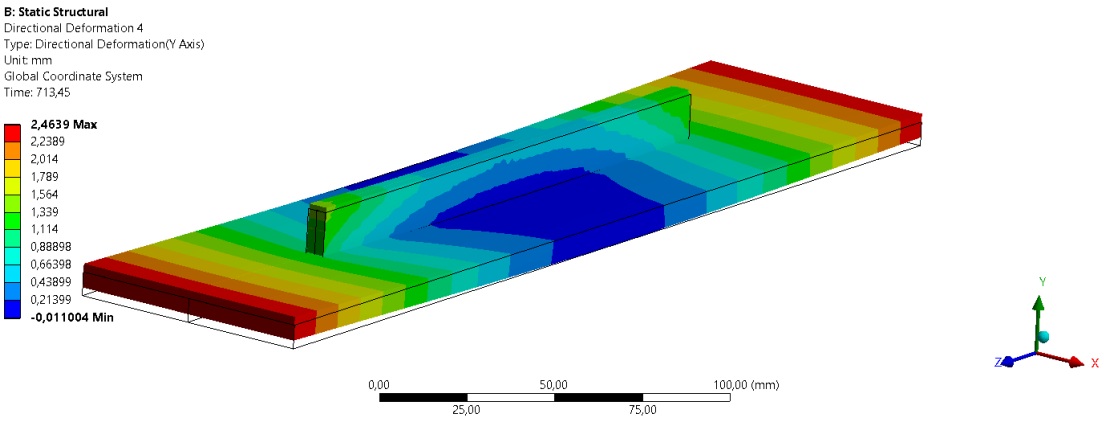


Figure 9. Distortion in the part base.

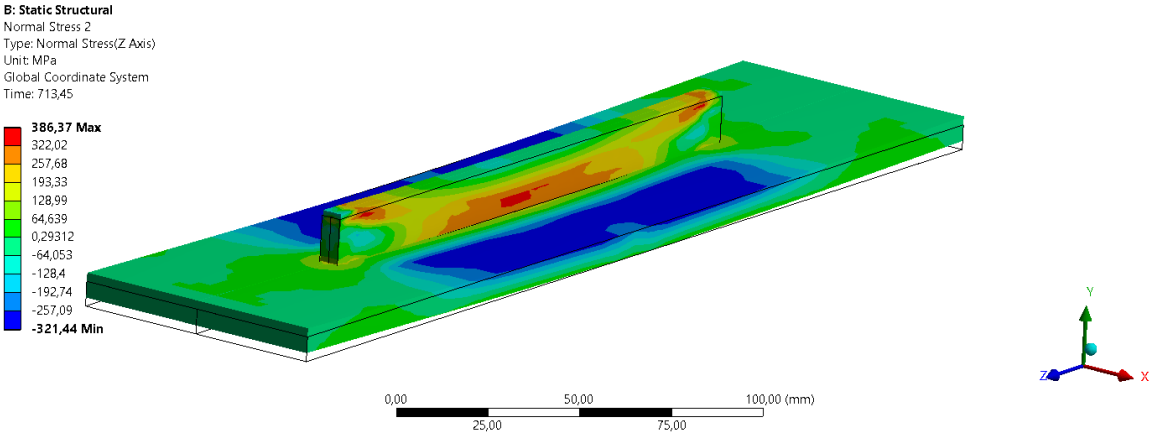


Figure 10. Longitudinal residual stress in the part base.

## 5. CONCLUSIONS

In this work a FEM model was presented for the thermomechanical analysis of a carbon steel wall built by WAAM. The criteria and parameters used to carry out this analysis were also presented in this work. Thereby, it was possible to obtain the temperature field in the part at each time step, as well as distortions and residual stresses. The validation of the numerical model was carried out through an experimental test reported in this work. Temperature and distortion values were compared at different points of the experimental test and numerical model.

The thermal analysis was validated by comparing the temperature history of different points on the flat base, close to the wall. The mechanical analysis was validated by comparing the final distortions at different points on the side of the flat base. The temperatures and distortions predicted in the numerical model are in agreement with the results obtained experimentally. The numerical model makes it possible to estimate the temperature and stress field at the flat base of the part throughout the entire process of material deposition and cooling. This analysis can be used to predict the influence of different manufacturing parameters, deposition and cooling strategies and restriction methods. The temperature distribution on the wall during the welding process was analyzed using infrared camera images. The physical complexity and the difficulty of accurately measuring the temperature of the weld pool compromise the validation of the numerical model in this region. The temperature values of the experimental and the simulation converges in regions far away from the weld pool.

In the manufacture of large parts, temperature accuracy in regions close to the heat source are less relevant than the computational cost of a mesh with many elements. For future work, it is possible to test simplified heat sources for these

cases. It is also possible to perform a sensitivity analysis of the mechanical model, verifying the application of temperature-independent material parameters.

## 6. ACKNOWLEDGEMENTS

The authors would like to thank the LABSOLDA Welding and Mechatronics Institute for providing the necessary equipment and assistance to carry out the experimental test. We would like to thank the researcher N. Portela for preparing, accompanying, and assisting in the experimental analysis as well.

Finally, the authors would like to thank FAPEU and Petrobras for funding this research within the research project of Alternative Welding Repair Processes.

## 7. REFERENCES

Arevalo, H.D.H., and Vilarinho, L.O., 2012. Desenvolvimento e avaliação de calorímetros por nitrogênio líquido e fluxo contínuo para medição de aporte térmico. *Soldagem & Inspeção*, *17*(3), 236–250.

Deng, D., 2009. FEM prediction of welding residual stress and distortion in carbon steel considering phase transformation effects. *Materials & Design*, *30*(2), 359–366.

Ding, D., Pan, Z., Cuiuri, D., and Li, H., 2015. Wire-feed additive manufacturing of metal components: technologies, developments and future interests. *The International Journal of Advanced Manufacturing Technology*, *81*(1), 465–481.

Ding, D., Zhang, S., Lu, Q., Pan, Z., Li, H., and Wang, K., 2021. The well-distributed volumetric heat source model for numerical simulation of wire arc additive manufacturing process. *Materials Today Communications*, *27*, 102430.

Ding, J., Colegrove, P., Mehnen, J., Ganguly, S., Sequeira Almeida, P. M., Wang, F., and Williams, S., 2011. Thermo-mechanical analysis of Wire and Arc Additive Layer Manufacturing process on large multi-layer parts. *Computational Materials Science*, *50*(12), 3315–3322.

Galeazzi, D., Silva, R. H. G. e., Viviani, A. B., Jaeger, P. R., and Schwedersky, M. B., 2022. Evaluation of thermal and geometric properties of martensitic stainless steel thin walls built by additive manufacturing cold metal transfer (CMT) processes. *The International Journal of Advanced Manufacturing Technology*, *120*(3), 2151–2165.

Ganeriwala, R. K., Hodge, N. E., and Solberg, J. M. 2021. Towards improved speed and accuracy of laser powder bed fusion simulations via multiscale spatial representations. *Computational Materials Science*, *187*, 110112.

Goldak, J., and Akhlaghi, M., 2005. Computer Simulation of Welding Processes. In J. A. Goldak & M. Akhlaghi (Eds.), *Computational Welding Mechanics* (pp. 16–69). Springer US.

Goldak, J., Chakravarti, A., and Bibby, M., 1984. A new finite element model for welding heat sources. *Metallurgical Transactions B*, *15*(2), 299–305.

Li, Y., Su, C., and Zhu, J., 2022. Comprehensive review of wire arc additive manufacturing: Hardware system, physical process, monitoring, property characterization, application and future prospects. *Results in Engineering*, *13*, 100330.

Lindgren, L.E., 2001. Finite Element Modeling and Simulation of Welding. Part 2: Improved Material Modeling. *Journal of Thermal Stresses*, *24*(3), 195–231.

Lindgren, L.E., 2006. Numerical modelling of welding. *Computer Methods in Applied Mechanics and Engineering*, *195*(48), 6710–6736.

Masubuchi, K., 1980. *Analysis of Welded Structures* (pp. 88–111). Pergamon.

Michaleris, P., and DeBiccari, A., 1997. Prediction of Welding Distortion. *Welding Journal*, 172–179.

Montevecchi, F., Venturini, G., Scippa, A., and Campatelli, G., 2016. Finite Element Modelling of Wire-arc-additive-manufacturing Process. *Procedia CIRP*, *55*, 109–114.

Murakawa, H., Deng, D., Ma, N., and Wang, J., 2012. Applications of inherent strain and interface element to simulation of welding deformation in thin plate structures. *Computational Materials Science*, *51*(1), 43–52.

Radaj, D., 1992. *Heat Effects of Welding: Temperature Field, Residual Stress, Distortion* (pp. 1–18). Springer Berlin Heidelberg.

Shan, X., Davies, C. M., Wangsdan, T., O'Dowd, N. P., and Nikbin, K. M., 2009. Thermo-mechanical modelling of a single-bead-on-plate weld using the finite element method. *International Journal of Pressure Vessels and Piping*, *86*(1), 110–121.

Szost, B., Terzi, S., Martina, F., Boisselier, D., Prytuliak, A., Pirling, T., Hofmann, M., and Jarvis, D., 2015. A comparative study of additive manufacturing techniques: Residual stress and microstructural analysis of CLAD and WAAM printed Ti–6Al–4V components. *Materials and Design*.

## 8. RESPONSIBILITY NOTICE

The authors are the only responsible for the printed material included in this paper.